

**Chapter 4: Ground-State Singlet $L_3Fe-(\mu-N)-FeL_3$ and $L_3Fe(NR)$
Complexes Featuring Pseudotetrahedral Fe(II) Centers**

The text in this chapter is reproduced in part with permission from:

Brown, S. D.; Peters, J. C. *J. Am. Chem. Soc.* **2005**, *127*, 1913.

Copyright 2004 American Chemical Society

4.1 Introduction

Low-coordinate iron sites that feature terminally bound or bridged nitride ligands may be relevant to various nitrogen reduction schemes.¹ For example, the report of an interstitial μ_6 -ligand (presumably a nitride) within the MoFe-cofactor of nitrogenase² has drawn recent attention to Fe-N-Fe structure types germane to biological nitrogen fixation.³ Schemes have also been forwarded to suggest that an N₂ scission process on hot iron surfaces might lead to surface-bound iron nitrides that are reactive toward hydrogen during the Haber-Bosch ammonia synthesis.⁴ In this broad context, it is noteworthy that synthetically well-defined molecular iron nitrides, whether terminal or bridging, are uncommon.^{5,6} For instance, there are presently no examples of bimetallic Fe-(μ -N)-Fe species if one restricts consideration to iron centers that feature coordination numbers lower than five. Moreover, terminal nitrides of iron, regardless of coordination number, are exceptionally rare.^{6,7} Well-defined, low-coordinate iron nitrides that can be thoroughly characterized are therefore of synthetic interest, and we have begun to undertake their systematic development.

As a preface to the current study, our laboratory has invested considerable effort in the synthesis and study of various monomeric pseudotetrahedral L₃Fe-N_x platforms to assess what range of N_x-type ligands, oxidation states, and redox processes might be accommodated by a single pseudotetrahedral iron site. Using tris(phosphino)borate ligands as the L₃ auxiliary,⁸ we have observed that an L₃Fe-N_x center can display a remarkable range of redox flexibility, supporting π -acidic N₂⁹ and π -basic nitride⁶ (N³⁻) at the extremes, but also a range of intermediate N_x-type ligands that include amide,¹⁰ imide,^{9,11} and diazenido.⁹ A characteristic feature of these L₃Fe-N_x species that feature

strong Fe-N_x π-bonding is their propensity to populate a low-spin ground-state electronic configuration. For instance, the complexes [PhBP^{*i*Pr}₃]Fe^{IV}≡N and [PhBP^{*i*Pr}₃]Fe^{III}≡N(1-Ad) are characterized by one σ and two π bonds at the Fe-N_x linkage and exhibit *S* = 0 and *S* = 1/2 ground states, respectively, despite the fact that the iron centers are pseudotetrahedral ([PhBP^{*i*Pr}₃] = [PhB(CH₂P^{*i*Pr}₂)₃]).¹²

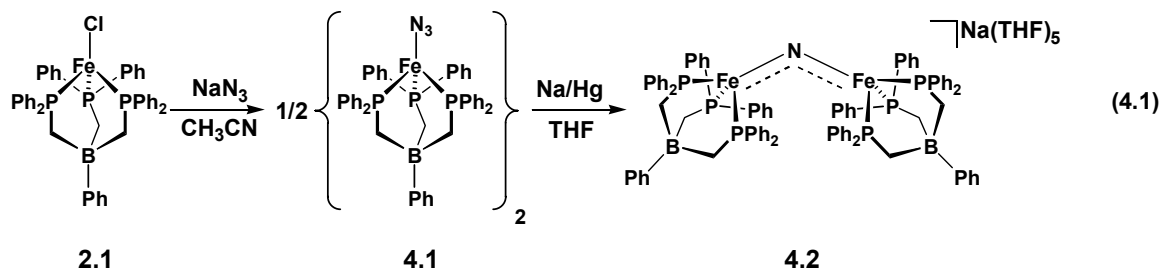
In this report, we describe a new bimetallic L₃Fe-N_x-FeL₃ complex in which the L₃ scaffold is the parent [PhBP₃] ligand ([PhBP₃] = [PhB(CH₂PPh₂)₃]),¹³ and the N_x ligand is a bridging nitride group. As alluded to above, previously prepared bridged nitride diiron systems have featured five- or six-coordinate iron centers in relatively high oxidation states (e.g., Fe^{III}(μ-N)Fe^{IV}, Fe^{IV}(μ-N)Fe^{IV}).⁵ The system described herein, [{[PhBP₃]Fe}₂(μ-N)][Na(THF)₅] (**4.2**), is distinct from these complexes with respect to the coordination number and the formal oxidation state of each of its iron centers. The divalent iron sites in **4.2** are pseudotetrahedral iron(II), and the complex is diamagnetic in solution even at room temperature. A related mononuclear Fe(II) complex can be prepared that features a bona fide low-spin ground-state, {[PhBP₃]Fe^{II}≡N(1-Ad)}{^{*n*}Bu₄N} (**4.3**). However, comparative spectroscopic data indicate that **4.2** is best described by two high-spin Fe(II) centers that exhibit such strong antiferromagnetic coupling that a singlet state is exclusively populated at 293 K.

4.2 Results and Discussion

Whereas the reaction between [PhBP^{*i*Pr}₃]FeCl and [Li][dbabh]¹⁴ (dbabh = 2,3:5,6-dibenzo-7-aza bicycle[2.2.1]hepta-2,5-diene) cleanly generates an amide intermediate, [PhBP^{*i*Pr}₃]Fe(dbabh), that subsequently decays to [PhBP^{*i*Pr}₃]Fe^{IV}≡N,⁶ the reaction between [PhBP₃]FeCl (**2.1**)¹¹ and [Li][dbabh] is ill-defined, and no evidence for a

terminally bound nitride species is observed. To examine N-atom transfer to this latter system, we focused on the installation of azide (N_3^-) as a suitable N^{3-} source.¹⁵

Access to the required iron(II) azide precursor is readily accomplished via metathesis between **2.1** and sodium azide in acetonitrile (Equation 4.1). Dissolution of yellow, paramagnetic **2.1** in CH_3CN gives rise to a red solution in which complete consumption of **2.1** is evident by ^1H and $^{31}\text{P}\{^1\text{H}\}$ NMR spectroscopy. The $^{31}\text{P}\{^1\text{H}\}$ NMR spectrum of this solution reveals a singlet at δ 44.5 ppm, consistent with the formation of a C_3 -symmetric solvento adduct that we formulate as $\{[\text{PhBP}_3]\text{Fe}(\text{CH}_3\text{CN})_3\}\{\text{Cl}\}$. A related species, $\{[\text{PhBP}_3]\text{Fe}(\text{CH}_3\text{CN})_3\}\{\text{PF}_6\}$, has been isolated and characterized.¹⁶ The ^1H NMR spectrum (CD_3CN) reveals, in addition to the major diamagnetic product, the presence of a minor paramagnetic species that we tentatively formulate as $[\text{PhBP}_3]\text{Fe}(\text{CH}_3\text{CN})(\text{Cl})$. A similar five-coordinate iron-containing species has been characterized with the $[\text{PhBP}^{i\text{Pr}}_3]$ ligand.^{12b} Upon addition of 1 equiv of $[\text{Na}][\text{N}_3]$ to a red acetonitrile solution of **2.1**, the gradual precipitation of purple solids occurs over a period of hours. Extraction of these solids with copious amounts of benzene and subsequent filtration through a pad of celite yields $\{[\text{PhBP}_3]\text{Fe}(\mu\text{-}1,3\text{-N}_3)\}_2$ (**4.1**) as a reddish-brown solid in 85% yield. Installation of a terminal azide functionality is readily confirmed by solution-state infrared spectroscopy due to the presence of a strong vibration at 2077 cm^{-1} .¹⁷ Repeating the synthesis with $[\text{Na}][^{15}\text{N}]\text{NNN}$ yields **4.1**- ^{15}N in which the azide



vibration is shifted to 2066 cm^{-1} . Dilute solutions of **4.1** are transparent yellow in color with optical data ($\lambda = 410\text{ nm}$, $\varepsilon = 700\text{ M}^{-1}\text{ cm}^{-1}$) similar to that observed for the monomeric chloride **2.1**. Evans method¹⁸ magnetic measurements on crystalline samples of **2** dissolved in C_6D_6 repeatedly afforded magnetic moments of $4.50 (\pm 0.04)\ \mu_{\text{B}}$, a value somewhat below the spin-only value of $4.89\ \mu_{\text{B}}$ for four unpaired electrons. Other pseudotetrahedral $[\text{PhBP}^{i\text{Pr}}_3]\text{Fe}(\text{II})$ complexes, for example, $[\text{PhBP}^{i\text{Pr}}_3]\text{FeMe}$, also exhibit moments below the spin-only value.¹⁹ We note that a monomer-dimer equilibrium process occurs for **4.1** in solution, as reflected by a color change from yellow to red upon cooling, and the dimeric form has been characterized in the solid state by X-ray diffraction and SQUID magnetometry.

Red crystals of **4.1** suitable for an X-ray diffraction experiment were grown via a benzene/petroleum ether vapor diffusion chamber, and its solid-state structure is shown in Figure 4.1. Azide **4.1** crystallizes in the triclinic crystal system with a benzene solvent molecule (omitted from Figure 1 for clarity) and features a dimeric $\text{Fe}_2(\mu\text{-}1,3\text{-N}_3)_2$ core that possesses a crystallographic center of symmetry.²⁰ The coordination geometry of each iron center is therefore identical and is best described as distorted square pyramidal ($\tau = 0.4$)²¹ in which N1, N3, P2, and P3 comprise the basal plane. As a result of the vacant coordination site trans to P1, the Fe-P1 bond distance of $2.1610(5)\ \text{\AA}$ is slightly shorter than that observed for Fe-P2 ($2.2279(6)\ \text{\AA}$) and Fe-P3 ($2.2101(6)\ \text{\AA}$). The N-N bond distances in each of the azide bridges are nearly identical at $1.181(2)\ \text{\AA}$ (N1-N2 and N1A-N2A) and $1.175(2)\ \text{\AA}$ (N2-N3A and N2A-N3).

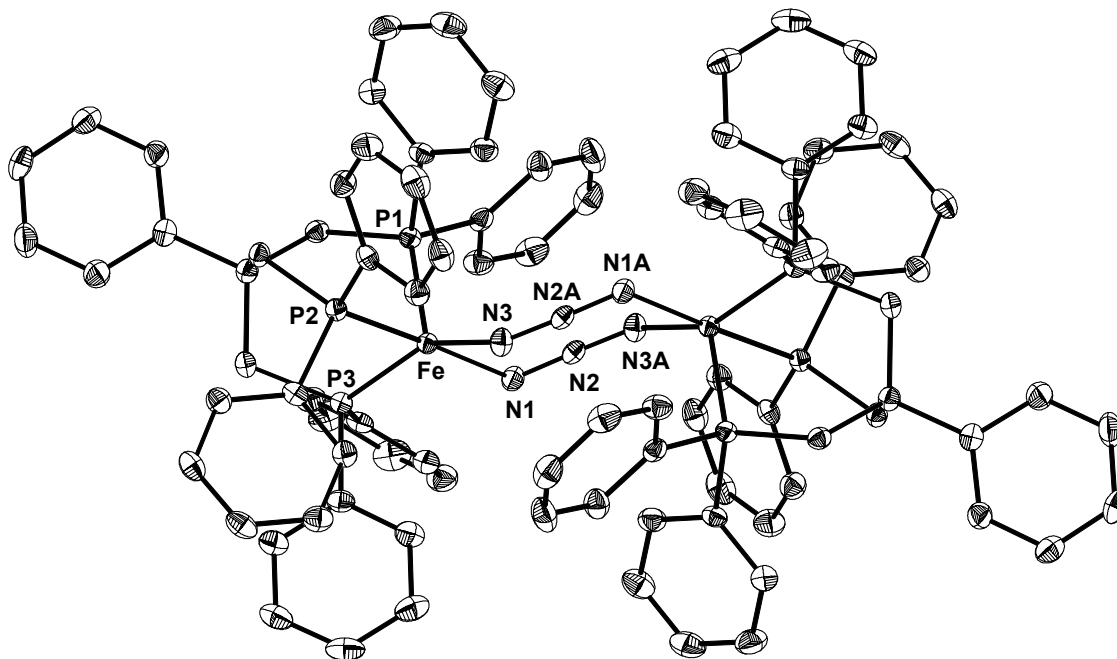


Figure 4.1. 50% thermal ellipsoid representation of $\{[\text{PhBP}_3]\text{Fe}(\mu\text{-}1,3\text{-N}_3)\}_2$ (**4.1**). All hydrogen atoms and a benzene solvent molecule have been removed for clarity. Selected bond lengths (Å) and angles (°): Fe-N1: 2.0107(15); Fe-N3: 1.9516(16); N1-N2: 1.181(2); N2-N3A: 1.175(2); Fe-P1: 2.1610(5); Fe-P2: 2.2279(6); Fe-P3: 2.2101(6); P1-Fe-P2: 89.37(2); P1-Fe-P3: 92.23(2); P1-Fe-N1: 94.52(5); P1-Fe-N3: 116.91(5); P2-Fe-P3: 89.88(2); N3-Fe-N1: 87.06(6); N1-Fe-P2: 175.64(5); N1-Fe-P3: 91.92(5); P3-Fe-N3: 150.84(5).

Solid-state magnetic susceptibility data for **4.1** were obtained from 4 to 290 K by SQUID magnetometry and are plotted, per dimeric unit, in Figure 4.2. The plot of χ_M^*T versus temperature (Figure 4.2 *top*) is consistent with ferromagnetic coupling as a marked increase in the value of χ_M^*T is observed as the sample is cooled. A maximum value of $8.31 \text{ cm}^3 \text{ K mol}^{-1}$ is observed at 40 K, and further cooling of the sample results in a decrease in the value of χ_M^*T , which is likely attributable to zero-field splitting.²² The

plot of μ_{eff} versus temperature (Figure 4.2 *bottom*) establishes a room-temperature magnetic moment of $4.3 \mu_{\text{B}}$ for **4.1**, while a maximum value of $8.2 \mu_{\text{B}}$ is observed at 40 K.

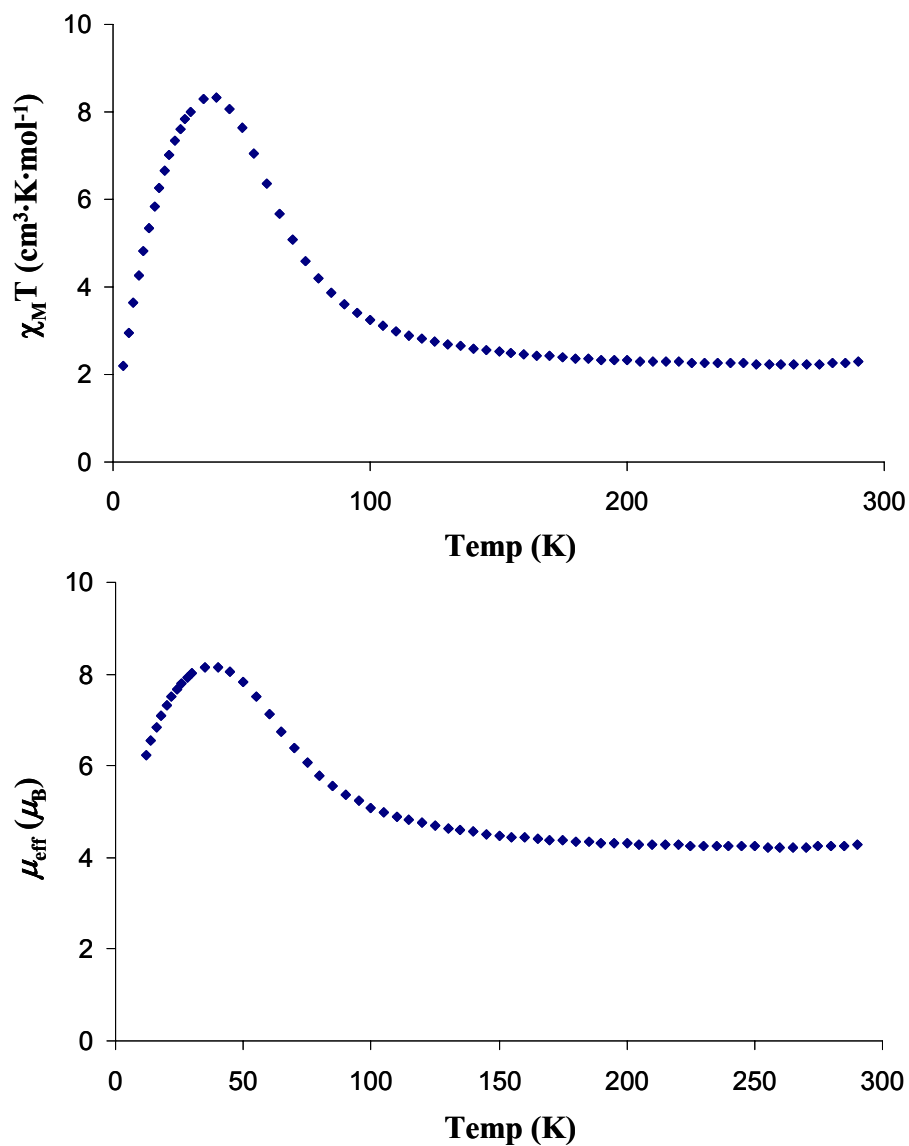


Figure 4.2. SQUID magnetometry data for **4.1** plotted *per dimeric unit* as (*top*) $\chi_M T$ versus temperature and (*bottom*) μ_{eff} versus temperature.

As depicted in Equation 4.1, the chemical reduction of **4.1** is readily accomplished in THF with 1 equiv of a 0.2 weight % Na/Hg amalgam. A darkening of the reaction solution is accompanied by the effervescence of gas almost immediately upon exposure of **4.1** to the amalgam. After the mixture was stirred at room temperature for 8 h, the major product of the reaction, $[\{\text{PhBP}_3\text{Fe}\}_2(\mu\text{-N})][\text{Na}(\text{THF})_5]$ (**4.2**), was isolated as a brown solid in ca. 50% yield. Crystals of **4.2** suitable for X-ray diffraction analysis were grown via a THF/hexanes vapor diffusion chamber, and its solid-state structure is shown in Figure 4.3A. Compound **4.2** crystallizes in the monoclinic crystal system with a free molecule of THF (omitted from Figure 4.3 for clarity). The nitride ligand was refined in two positions (Figure 4.3 B and C) and modeled satisfactorily with a population ratio of 1.86 to 1. Repeating the X-ray diffraction experiments on several independently synthesized and crystallized samples consistently afforded data in which the nitride ligand was located in two positions, including samples in which the sodium cation had been exchanged for a $n\text{Bu}_4\text{N}^+$ cation. Combustion analysis data for **4.2** is consistent with a single $\mu\text{-N}$ ligand.

In contrast to precursor **4.1**, each iron center in the anion of **4.2** is crystallographically unique and exhibits a geometry that is best described as distorted tetrahedral. The relatively short Fe-N_{av} bond distance of 1.70 Å for both positions of the nitride ligand is consistent with multiple bonding character.^{9,11,23} One of the dramatic structural differences between **4.2** and other literature examples of diiron $\mu\text{-nitride}$ systems concerns the Fe-N-Fe bond angle of **4.2**, which averages 135° for either position of the nitride ligand.²⁴ All previous examples of structurally characterized bridging iron nitrides feature linear Fe-N-Fe linkages.⁵ In fact, to the best of our knowledge, the only

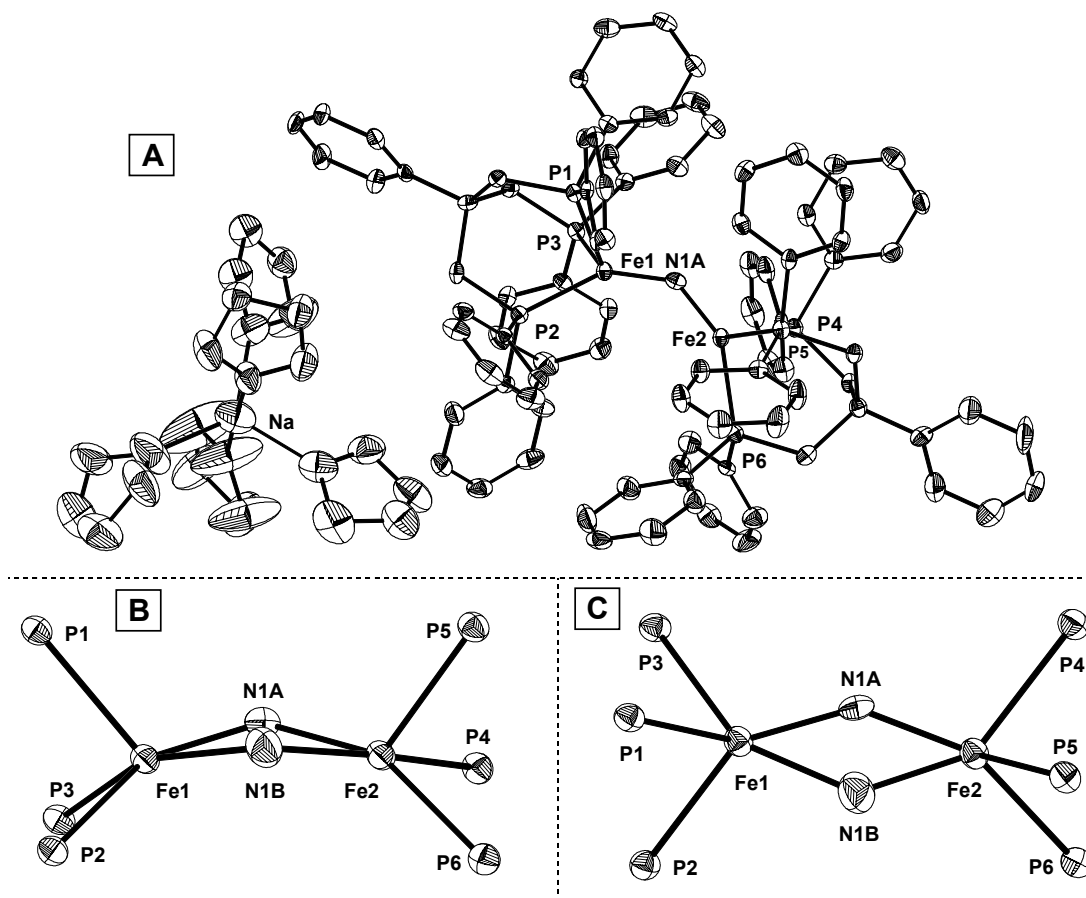


Figure 4.3. (A) 50% thermal ellipsoid representation of $[\{\text{PhBP}_3\}\text{Fe}]_2(\mu\text{-N})[\text{Na}(\text{THF})_5]$ **4.2** showing only the more populated position of the disordered nitride ligand. A free molecule of THF has been omitted for clarity. Selected bond distances (Å) and angles ($^\circ$): Fe1-N1A: 1.675(5); Fe2-N1A: 1.705(5); Fe1-Fe2: \sim 3.13; Fe1-P1: 2.2295(10); Fe1-P2: 2.2338(10); Fe-P3: 2.2127(10); Fe2-P4: 2.2299(10); Fe2-P5: 2.2106(10); Fe2-P6: 2.2534(10); Fe1-N1A-Fe2: 135.9(3); P1-Fe1-P2: 92.10(4); P1-Fe1-P3: 88.83(4); P2-Fe1-P3: 90.79(4); P2-Fe1-N1A: 143.93(16); P1-Fe1-N1A: 112.69(14); P3-Fe1-N1A: 114.45(15). (B) Side view of the Fe1-N-Fe2 core of **4.2** showing both positions of the disordered nitride ligand. (C) Top view of the Fe1-N-Fe2 core of **4.2** showing both positions of the disordered nitride ligand.

other report of a mono-bridged bimetallic nitride species featuring an appreciably bent M-N-M linkage is that from Floriani and co-workers in which the anion of [$\{p\text{-}^t\text{Bu-calix[4]-(O)}_4\}_2\text{Nb}_2(\mu\text{-N})\}[\text{Na}(\text{TMEDA})_2]$ (TMEDA = N,N,N',N' -tetramethylethylenediamine) was reported to have a bond angle of $145.2(1)^\circ$.²⁵ This type of bent structure is reminiscent of $\text{R}_3\text{P}=\text{N}=\text{PR}_3$ cations, which feature bridging nitride ligands sandwiched by 4-coordinate phosphorus centers. Examples of $\text{R}_3\text{P}=\text{N}=\text{PR}_3$ cations in which the P-N-P bond angle is approximately 135° and the two N-P bond distances are similar, but crystallographically distinct, have been reported.²⁶ Direct Fe-Fe bonding interactions within **4.2** are unlikely given their separation by ca. 3.13 \AA .²⁷

Characteristic NMR resonances for triply recrystallized samples of nitride **4.2** are observed by ^1H , $^{31}\text{P}\{^1\text{H}\}$, and ^{15}N NMR spectroscopy (a 50% ^{15}N -enriched sample of **4.2** may be generated from the reduction of **4.1**- ^{15}N), consistent with the assignment of a singlet ground state. The $^{31}\text{P}\{^1\text{H}\}$ spectrum features a singlet at $\delta 58.0$ ppm, and the ^1H NMR spectrum in THF- d_8 displays, in addition to several equivalents of THF due to the sodium cation, one set of diamagnetic resonances corresponding to the $[\text{PhBP}_3]$ ligand. A singlet at $\delta 801$ ppm (versus NH_3 at $\delta 0$ ppm) in the ^{15}N NMR spectrum of **4.2** confirms the presence of the nitride functionality. We were unable to resolve ^{15}N - ^{31}P coupling, similar to the case of the terminal nitride derivative $[\text{PhBP}^{i\text{Pr}}_3]\text{Fe}^{\text{IV}}\equiv\text{N}^6$ where an ^{15}N NMR signal was observed at $\delta 952$ ppm. The downfield nature of the nitride resonance in comparison with other mono-bridged systems²⁸ likely reflects a paramagnetic contribution to the chemical shift from the antiferromagnetically coupled high-spin ferrous centers (*vide infra*). In accord with the assignment of a diamagnetic ground state, nitride **4.2** is X-band EPR silent at 4 K as a glassy 1-methyltetrahydrofuran solution.

Two limiting electronic descriptions for complex **4.2** need to be considered. It can be electronically described by two localized low-spin $S = 0$ Fe(II) centers, or alternatively as a fully delocalized system that features two high-spin $S = 2$ Fe(II) centers that are sufficiently antiferromagnetically coupled that a singlet ground state is populated even at room temperature. In accord with the latter description, Holland, Munck, and co-workers recently reported a sulfido-bridged diiron(II) compound that features paramagnetic solution chemical shifts in the ^1H NMR spectrum at room temperature, but is assigned to an $S = 0$ ground state due to antiferromagnetic coupling on the basis of low-temperature Mossbauer data.²⁹ In addition, Wieghardt, Trautwein, and co-workers have described an interesting $\text{Fe}^{\text{IV}}(\mu\text{-N})\text{Fe}^{\text{IV}}$ complex that is diamagnetic in solution at room temperature, suggesting strong antiferromagnetic coupling and a lower $|J|$ value limit of 250 cm^{-1} .^{5a}

To further examine this issue, we prepared a mononuclear d^6 iron(II) complex exhibiting a related pseudotetrahedral geometry with one π -bonded N_x type linkage for comparison. This complex, $\{[\text{PhBP}_3]\text{Fe}^{\text{II}}\equiv\text{N}(1\text{-Ad})\}\{\text{}^n\text{Bu}_4\text{N}\}$ (**4.3**), is diamagnetic and clearly establishes that an isolated pseudotetrahedral Fe(II) center can adopt a low-spin ground-state electronic configuration. Complex **4.3** was easily prepared by Na/Hg amalgam reduction of $S = 1/2$ $[\text{PhBP}_3]\text{Fe}^{\text{III}}\equiv\text{N}(1\text{-Ad})$ (**2.12**), followed by the addition of $[\text{}^n\text{Bu}_4\text{N}][\text{Br}]$. The trivalent imide precursor **2.12** was itself readily prepared by the addition of 1-adamantyl azide to $[\text{PhBP}_3]\text{Fe}(\text{PPh}_3)$ (**2.4**), a procedure analogous to that used in the preparation of the related imide $[\text{PhBP}_3]\text{Fe}^{\text{III}}\equiv\text{N}(p\text{-tolyl})$ (**2.5**).¹¹ Complex **4.3** represents what is, to the best of our knowledge, the only reported example of a d^6 iron imide³⁰ and is moreover the first example of a monomeric, pseudotetrahedral $S = 0$ Fe(II) complex.

The solid-state structures of both **4.3** and **2.12** have been determined for comparison with one another and with nitride **4.2**, their core structures are shown in Figure 4.4. Most striking is the overall similarity of the structures of **4.3** and **2.12** at

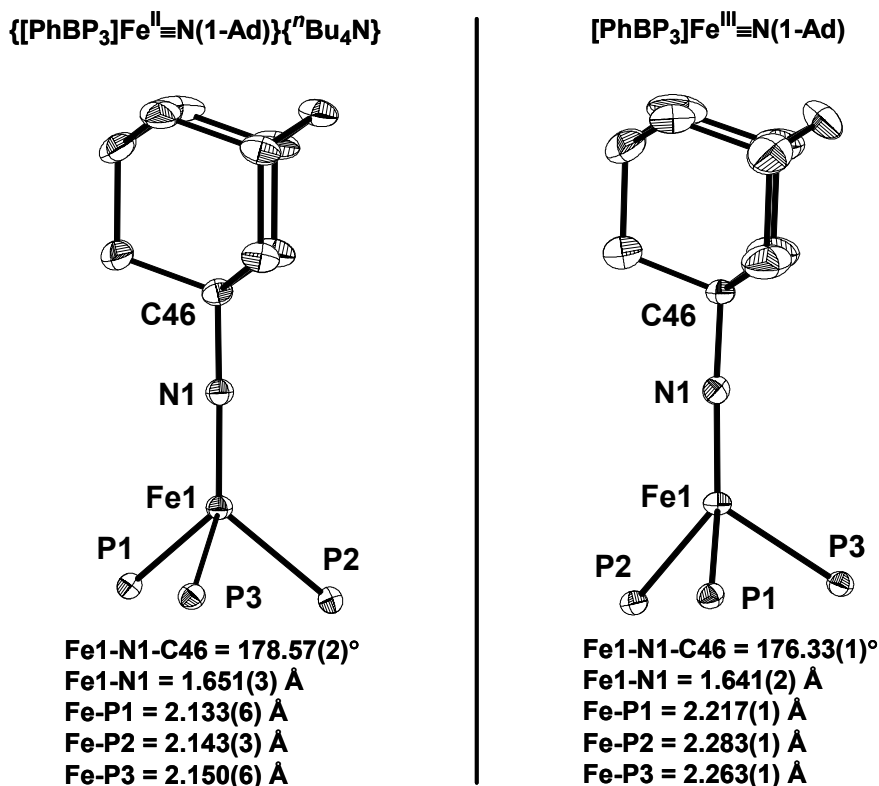


Figure 4.4. Solid-state molecular structures of **4.3** (*left*) and **2.12** (*right*) showing 50% displacement ellipsoid representations for the P₃Fe≡N(1-Ad) core. For **4.3**, a THF solvent molecule and the ⁿBu₄N⁺ cation have been removed for clarity. Selected bond lengths and angles are highlighted within the figure.

the Fe1-N1-C46 linkage, with respect to both the Fe1-N1 bond distance and the Fe1-N1-C46 bond angle, despite their different spin states. Given this similarity, a structural distinction worth noting is that the average Fe-P bond distances in the divalent anion of **4.3** are ca. 0.1 Å shorter than the average of the Fe-P bond distances for neutral, trivalent **2.12**. This difference is somewhat counterintuitive and may reflect the presence of an

unpaired spin in the case of **2.12**, although this explanation is unsatisfying given the predominantly nonbonding nature of the orbital that would house the unpaired electron (d_{xy} or $d_{x^2-y^2}$, vide infra). An alternative possibility to further consider is that the anion of **4.3** more strongly π -back-bonds into σ^* orbitals of the appropriate symmetry from the [PhBP₃] ligand than for the case of **2.12** by virtue of its d^6 (versus d^5) electronic configuration.³¹ This scenario would give rise to shorter Fe-P interactions. Also consistent with a π -back-bonding argument is the observation that the P-C bonds of anionic **4.3** are, on average, 0.016 Å longer than those for neutral **2.12**. A similar phenomenon has been observed for the complex [(PP₃)Fe(C≡CPh)][BPh₄] (PP₃ = P(CH₂CH₂PPh₂)₃),³² in which the one-electron reduction of this species induces a contraction of the Fe-P bond distances by an average of 0.09 Å. The authors also attributed this structural anomaly to π -back-bonding. These explanations notwithstanding, the magnitude between the respective Fe-P bond distances in **4.3** and **2.12** is noteworthy.

The average of the Fe-N bond distances in **4.2** is approximately 0.05 Å longer than that observed for **4.3** and **2.12**. Additionally, the Fe-P bond distances observed for **4.2** (Fe-P_{avg.} = 2.228 Å) are intermediate to those observed for the structures of **4.3** (Fe-P_{avg.} = 2.142 Å) and **2.12** (Fe-P_{avg.} = 2.254 Å). By contrast, the recently communicated high-spin Fe(II) amide complex [PhBP₃]Fe(N(H)-*p*-tolyl)(**3.1**)¹⁰ features diminished π -bonding character at the Fe-N linkage in comparison to **4.2**, **4.3**, and **2.12** and exhibits expanded Fe-N and Fe-P distances due to its preferred $S = 2$ ground-state electronic configuration (Fe-N = 1.913 (2) Å, Fe-P_{avg.} = 2.424 Å). On the basis of these structural considerations, the tabulation of charges for **4.2**, and the fact that it exhibits a

diamagnetic ground state, it might seem most reasonable to assign each of the iron centers of **4.2** as localized and low-spin Fe(II). A comparison of the electronic absorption spectra for compounds **2.1**, **4.2**, and **4.3**, however, seems to suggest that this is not the best description.

Electronic absorption spectra for compounds **2.1**, **4.2**, and **4.3** were collected from 350 to 2000 nm at room temperature in THF-*d*₈, and the resulting spectra are shown in Figure 4.5. Chloride **2.1** (Figure 4.5, inset), which represents a classic example of high-spin iron(II), exhibits an absorption feature at 1285 nm (7782 cm⁻¹, ε = 185 M⁻¹ cm⁻¹) that is reflective of its expected low-energy d-d transitions.³³ The d-d transitions of similar energy are not expected for a low-spin iron(II) center due to a large HOMO-LUMO gap, nor are charge-transfer transitions, which would be expected to occur at much higher

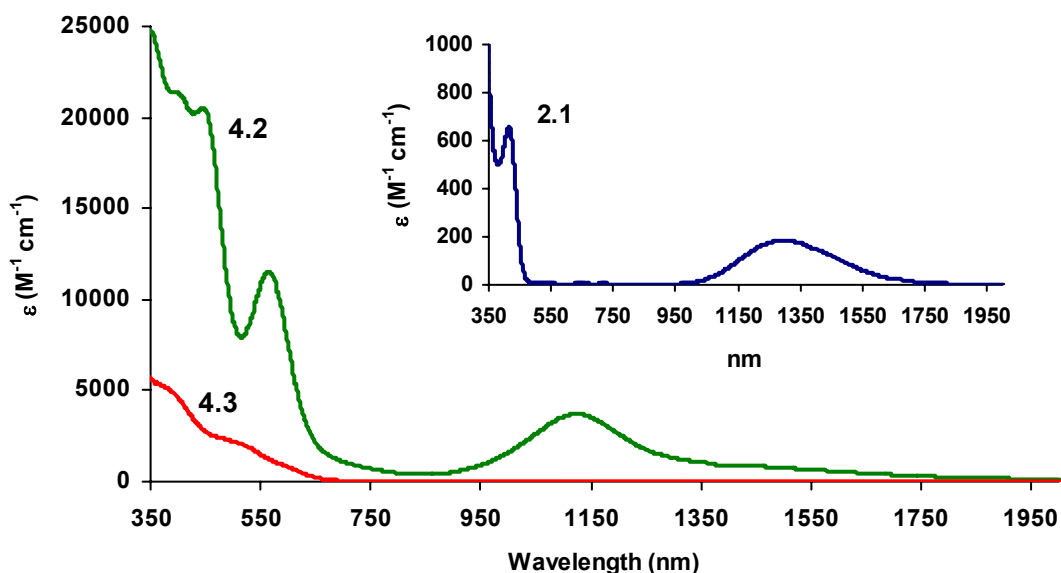


Figure 4.5. Electronic absorption spectrum of **2.1** (inset, blue), **4.2** (green), and **4.3** (red) in THF-*d*₈.

energy. Indeed, no d-d type or charge-transfer type transitions are observed in the NIR region of the spectrum for the rigorously low-spin Fe(II) imide **4.3**; a feature at ca. 510 nm ($19\,608\text{ cm}^{-1}$, $\epsilon = 2112\text{ M}^{-1}\text{ cm}^{-1}$) is likely reflective of an LMCT transition. Inspection of the NIR region of the spectrum for complex **4.2**, however, reveals a very broad and intense feature centered at approximately 1120 nm (8929 cm^{-1} , $\epsilon = 3720\text{ M}^{-1}\text{ cm}^{-1}$). This feature, which we assume arises from a charge-transfer transition associated with the bridged nitride ligand, displays an easily discernible shoulder on its low-energy side that reflects the low-energy d-d transitions characteristic of high-spin Fe(II) and observed in **2.1**. Curve-fitting of the NIR data for **4.2** from 850 to 2000 nm using GRAMS v.3.2 (Thermo Galactic, see Supporting Information) resolves the two features into a transition centered at 1120 nm (8929 cm^{-1} , $\epsilon = 2740\text{ M}^{-1}\text{ cm}^{-1}$) and one centered at 1266 nm (7900 cm^{-1} , $\epsilon = 943\text{ M}^{-1}\text{ cm}^{-1}$).

It is interesting to contemplate the cause of the low-spin configurations in complexes **4.2** and **4.3**. According to the d-orbital splitting scheme that we have previously used to describe the d^6 cobalt imide complex $[\text{PhBP}_3]\text{Co}\equiv\text{N}(p\text{-tolyl})$,^{13b} an appropriate electronic configuration for the simplest case, d^6 **4.3**, is $(d_z^2)^2(d_{xy}, d_x^2-y^2)^4(d_{xz}, d_{yz})^0$. Under idealized C_{3v} symmetry, these d-orbitals transform as $a_1 + 2e$. The d_z^2 orbital is expected to lie low in energy, very close to the nearly degenerate pair of d-orbitals that are oriented perpendicular to the Fe-N bond vector. A DFT calculation on the slightly simplified complex $\{[\text{PhBP}_3]\text{Fe}\equiv\text{N}(t\text{Bu})\}^-$ provides a minimized geometrical (Figure 4.6A) and electronic structure fully consistent with this view. As shown in Figure 4.6B, a two-over-three splitting diagram is obtained in which d_z^2 , d_{xy} , and $d_x^2-y^2$ are nearly degenerate and non-bonding, and a pair of unoccupied d_{xz} , d_{yz} orbitals that are both

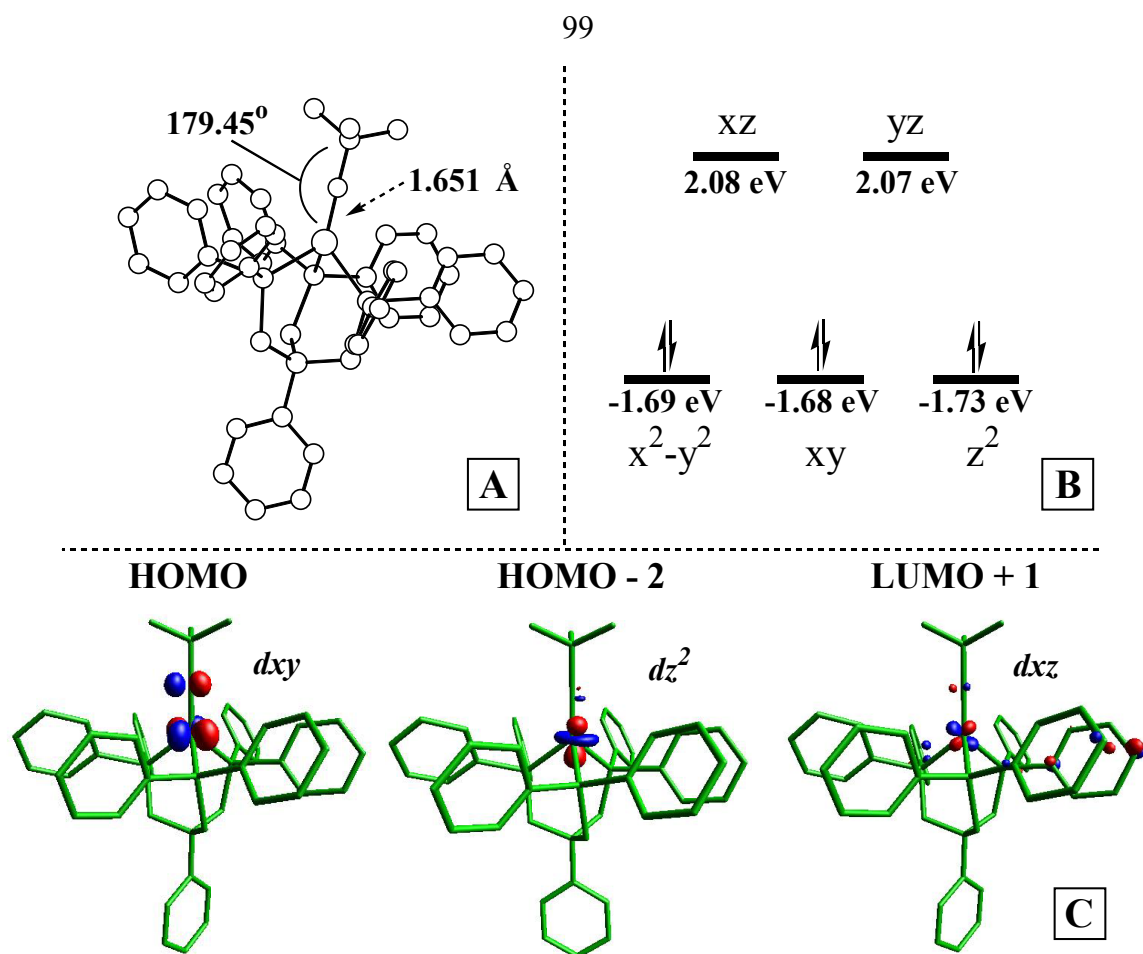


Figure 4.6. (A) Theoretically predicted geometry and (B) electronic structure (DFT, JAGUAR 5.0, B3LYP/LACVP**) for $S = 0$ $\{[\text{PhBP}_3]\text{Fe}\equiv\text{N}(\text{tBu})\}^-$. (C) Lobal representations of the highest occupied molecular orbital (HOMO), the orbital of d_{z^2} parentage (HOMO - 2), and the dxz orbital (LUMO + 1). Structural parameters: Fe-P = 2.209, 2.213, 2.213 Å; Fe-N = 1.651 Å; Fe-N-C = 179.45°; N-Fe-P = 125.08, 125.39, 125.63°; P-Fe-P = 89.72, 89.88, 89.97°.

σ^* and π^* in character lie at much higher energy. The calculation predicts the orbital of d_{z^2} parentage to lie lowest in energy (HOMO - 2), and the HOMO is therefore predicted to be either d_{xy} or $d_{x^2-y^2}$. Lobal representations for the HOMO, HOMO - 2, and LUMO + 1 orbitals are shown in Figure 4.6C. Hypothetical removal of one electron from this system

to generate Fe(III) is expected to give rise to a doublet ground-state species, which is observed for imide **2.12** ($\mu_{\text{eff}} = 1.98 \mu_{\text{B}}$). Because the electron is removed from an essentially nonbonding orbital, little structural change is expected at the Fe-N-C linkage, fully consistent with the solid-state structures of **4.3** and **2.12**. That the Fe-P bond distances in fact contract on reducing **2.12** to **4.3** is not as readily explained (*vide supra*).

The comparative cyclic voltammetry of **4.2** and **2.12** is of obvious interest and has been studied in THF (Fc/Fc⁺, 0.30 M [ⁿBu₄N][PF₆], 50 mV/s; Fc = ferrocene). The data acquired are shown in Figure 4.7. Inspection of the electrochemical response of **4.2** reveals an irreversible oxidative wave at -350 mV, a fully reversible redox process centered at -1340 mV, and another redox process at -2520 mV that appears to be quasi-reversible. The two redox events observed at the more positive potentials are strikingly

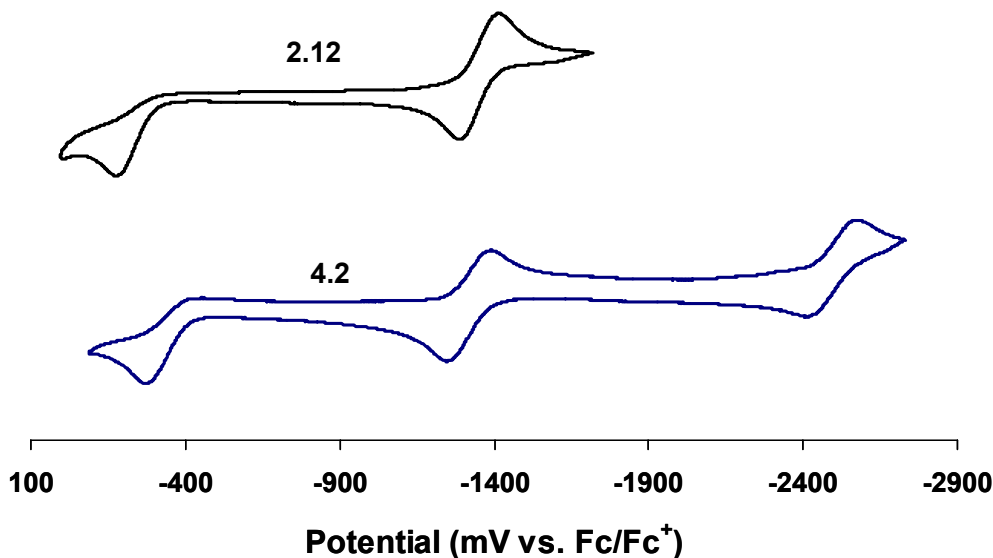
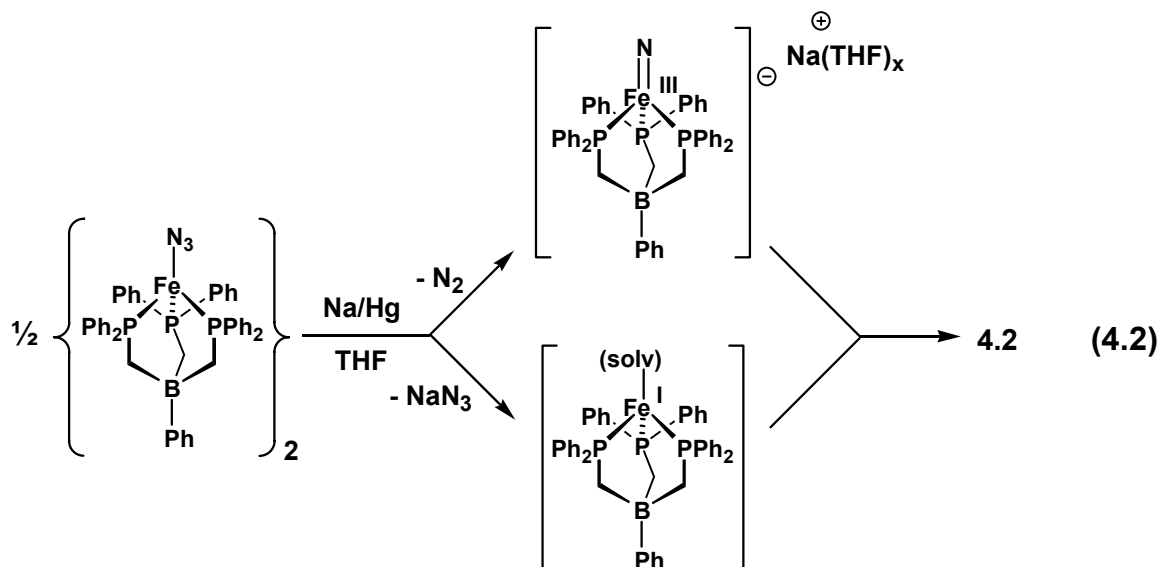


Figure 4.7. Cyclic voltammetry of [PhBP₃]Fe^{III}≡N(1-Ad) (**2.12**), top, and [{[PhBP₃]Fe}₂(μ-N)][Na(THF)₅] (**4.2**), bottom. Experimental parameters: 2.0 mM analyte, 0.30 M [ⁿBu₄N][PF₆] electrolyte, scan rate = 50 mV/s.

similar to those observed for **2.12**. In a previous communication, we have reported that a reversible $\text{Fe}^{\text{III/II}}$ redox process is available for $[\text{PhBP}_3]\text{Fe}^{\text{III}}\equiv\text{N-}p\text{-tolyl}$,¹¹ and the reversible wave centered at -1315 mV in the cyclic voltammogram of **2.12** is consistent with this picture and with the fact that this species can be chemically reduced to produce anionic **4.3**. The irreversible wave in the cyclic voltammogram of **2.12** has a peak maximum at -130 mV. We presume that this step represents an oxidation to generate a highly unstable “[PhBP_3] $\text{Fe}^{\text{IV}}\equiv\text{N(1-Ad)}^+$ ” species, or constitutes an oxidation of the borate ligand. We suggest that the reversible wave centered at -1.3 V in the cyclic voltammogram of **4.2** corresponds to an $\text{Fe(III)Fe(II)/Fe(II)Fe(II)}^-$ redox process. Several assignments are possible for the irreversible wave at -350 mV. It may correspond to an Fe(III)/Fe(IV) redox event at a single iron center consistent with the picture put forth for **2.12**, to an $\text{Fe(III)Fe(II)/Fe(III)Fe(III)}^+$ redox process, or to oxidative degradation of a borate ligand. The reduction wave at low potential (-2.5 V) is interesting and is not observed for complex **2.12**. This wave is suggestive of an $\text{Fe(II)Fe(II)}^-/\text{Fe(II)Fe(I)}^{2-}$ redox process in which the resulting reduced iron species appears to be relatively unstable under the conditions of the electrochemical experiment, as the anodic wave decreases and eventually vanishes when this redox event is isolated and cycled multiple times. Synthetic examination of this system using chemical reductants and oxidants may offer a better understanding of these redox events.

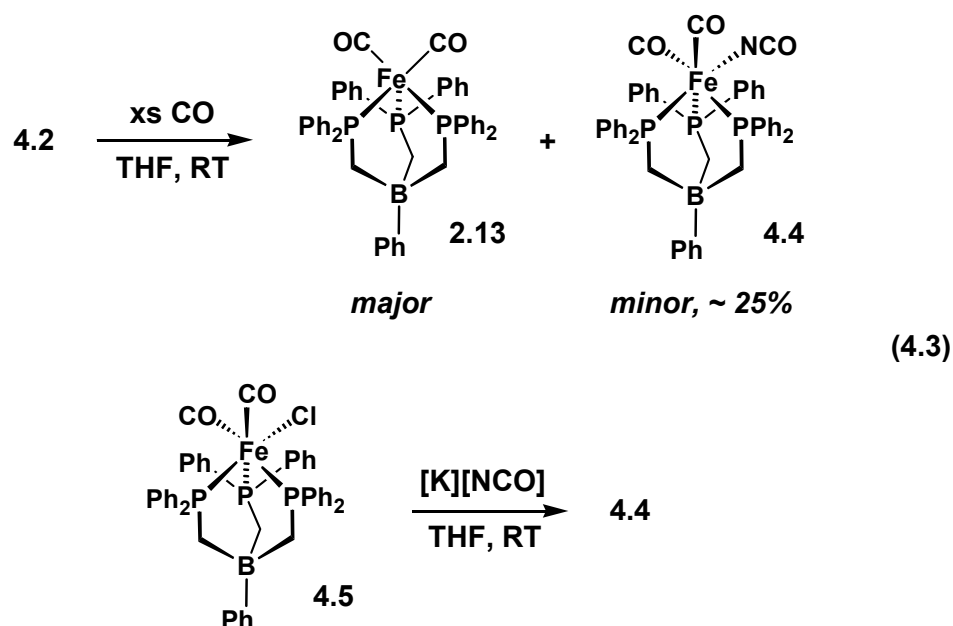
The mechanism concerning the conversion of **4.1** to **4.2** deserves some consideration. Due to the heterogeneous reaction and the paramagnetic nature of the precursor complex and presumable intermediates, it is a difficult system to probe experimentally. As shown in Equation 2, we presume that Na/Hg amalgam reduction of



4.1 to its corresponding anion releases N_2 gas, consistent with the observation of rapid effervescence. A plausible iron byproduct from N_2 release is the anionic nitride species “[$\text{PhBP}_3\text{Fe}^{\text{III}}(\text{N})$] $^-$.” Based upon the DFT calculations we have used to explore the electronic nature of a structurally related species, [$\text{PhBP}^{i\text{Pr}}_3\text{Fe}^{\text{IV}}\equiv\text{N}$],⁶ a single unpaired electron would populate a high-lying a_1 orbital featuring significant Fe-N σ^* character in [$\text{PhBP}_3\text{Fe}^{\text{III}}(\text{N})$] $^-$. This electronic situation should render the putative species highly reactive. It is therefore reasonable to suspect that if generated intermittently, such a species might attack the iron center of a secondary molecule of **4.1** to displace azide, or might attack the azide ligand itself.³⁴ Both of these scenarios have been suggested by Summerville and Cohen in the context of the photolysis products of a tetraphenylporphyrinatoiron(III) azide,^{5c} and also by Wieghardt, Trautwein, and co-workers.^{5a} We note that repeating the reduction of **4.1** in the presence of excess PPh_3 results in the formation of a substantial quantity of the previously reported Fe(I) complex [$\text{PhBP}_3\text{Fe}(\text{PPh}_3)$] (**2.4**),¹¹ in addition to nitride **4.2**. Because complex **4.1** itself does not react with PPh_3 , it appears likely that PPh_3 traps an Fe(I) source that is generated *in situ*.

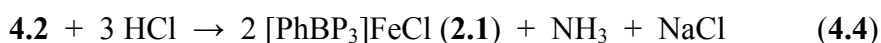
We can therefore put forth the notion that “[PhBP₃]Fe^{III}(N)]⁻” rapidly condenses with an “[PhBP₃]Fe^I(solv)” species to form isolable **4.2**, but the speculative nature of this suggestion needs to be underscored. One way to identify {[PhBP₃]Fe^{III}(N)]⁻ as an intermediate would involve trapping it by addition of an appropriate electrophile. Accordingly, we have tried to reduce the azide precursor **4.1** in the presence of trimethylsilyl chloride. While we do not know the nature of the reaction products, it is quite clear from spectroscopic data that [PhBP₃]Fe^{III}(NSiMe₃), the simplest product we might expect to form via metathesis (and elimination of NaCl and N₂), is not among these products.

An intriguing possibility was that addition of CO would lead to disproportionation of the system with liberation of [PhBP₃]Fe(CO)₂ (**2.13**)¹¹ and the elusive nitride species “[PhBP₃]Fe^{III}(N)]⁻” to which we have alluded to above. Exposure of **4.2** to an atmosphere of CO results in its instantaneous consumption (Equation 4.3), but the major product of the reaction proved to be the Fe^I dicarbonyl, **2.13**. A second iron-containing product, present in ca. 25% yield, was identified as the diamagnetic iron(II) isocyanate



complex $[\text{PhBP}_3]\text{Fe}(\text{CO})_2(\text{NCO})$ (**4.4**), a presumed product of nitride capture. The identity of diamagnetic **4.4** was readily ascertained by comparison of the crude spectral data (IR, ^1H , and $^{31}\text{P}\{^1\text{H}\}$) from the reaction with that of an independently prepared sample of **4.4** generated by the reaction between $[\text{PhBP}_3]\text{Fe}(\text{CO})_2\text{Cl}$ (**4.5**) and $[\text{K}][\text{NCO}]$. We have not identified the fate of the sodium cation in this reaction, but it is worth noting that, based upon the electronic structure considerations mentioned above for “ $[\text{PhBP}_3]\text{Fe}^{\text{III}}(\text{N})\}^-$,” we would expect it to be a powerful reductant if generated as an intermediate. Its oxidation product, $[\text{PhBP}_3]\text{Fe}^{\text{IV}}\equiv\text{N}$, should be susceptible to attack by CO to produce isolable **4.4**.³⁵ While it is unclear which species serves as the formal electron acceptor in the production of **4.4**, $[\text{PhBP}_3]\text{Fe}(\text{CO})_2$ and **4.4** are the only iron-containing products observed in the reaction.

While more comprehensive reactivity studies are in the offing, we wish to note that the (μ -N) ligand of **4.2** can serve as a source of NH_3 upon exposure to acid (Eq 4.4). Thus, the addition of 3 equiv. of HCl to a THF solution of **4.2** at $-35\text{ }^\circ\text{C}$ released NH_3 in good yield (two independent experiments provided NH_3 in yields of 80% and 95%),^{6,36} along with the chloride complex **2.1** as the predominant iron-containing byproduct (>80%). The yield of NH_3 was determined by vacuum transfer of the reaction volatiles into an ethereal solution containing HCl, which results in the precipitation of ammonium chloride. Subsequent isolation and quantification of the $[\text{NH}_4][\text{Cl}]$ salt was accomplished by NMR spectroscopy in $\text{DMSO-}d_6$ using a ferrocene integration standard.⁶ It is of future interest to add fewer proton equivalents, and perhaps H-atom equivalents (H^+/e^-) to **4.2** to



try to elucidate the other protonated forms of the system prior to NH_3 release (e.g., $\text{Fe}^{\text{II}}(\mu\text{-NH})\text{Fe}^{\text{II}}$ and $\text{Fe}^{\text{II}}\text{-NH}_2 + \text{Fe}^{\text{II}}\text{Cl}$).

4.3 Conclusions

The bimetallic bridged nitride complex **4.2** is unique in several regards. Foremost among these are the low coordination number and the low oxidation state of each of its two iron centers, and its severely bent Fe-N-Fe linkage. These features are unprecedented for bimetallic bridged iron nitrides and are very uncommon to bimetallic bridged nitrides more generally. Spectroscopic data for **4.2** suggest the presence of two high-spin ferrous centers that are sufficiently coupled to provide a singlet ground state even at room temperature.

While bridged iron nitride species are relatively rare, they may be important to nitrogen fixation schemes. As mentioned at the outset, it is interesting to recall the recent finding that the FeMo-cofactor of nitrogenase contains an interstitial light atom, presumably a nitride, surrounded by six pseudotetrahedral iron centers.² While this revised cofactor structure does little to clarify the mechanism of biological N_2 reduction, it at least calls attention to a possible role for relatively low-valent, low-coordinate Fe-(μ -N)-Fe linkages within the active site of the enzyme.³ Likewise, similar structural motifs may be relevant to the industrial synthesis of ammonia mediated by catalytically active, low-valent iron sites.⁴ While these suggestions remain highly speculative due to the absence of structural data during catalytic turnover conditions, the bimetallic nitride we have described at least provides chemical support for well-defined, low-valent μ -iron nitride systems. Specifically, our study shows that low-valent iron(II) centers are able to support bridging μ_2 -nitride ligands, in this case with pseudotetrahedral systems supported

by relatively soft phosphine donors. The μ_2 -nitride functionality can serve a structural role under reducing chemical conditions. The cyclic voltammetry of **4.2**, shown in Figure 4.7, adequately illustrates this point by revealing a pseudo-reversible $\text{Fe(II)Fe(II)}^-/\text{Fe(II)Fe(I)}^{2-}$ reduction process at low potential. It is of further note that the μ_2 -nitride ligand can serve as a source of NH_3 upon addition of protons.

Conceptually replacing one of the "[PhBP₃]Fe(II)" units in the anion of **4.2** with an organic moiety results in a mononuclear, anionic iron(II) imide. We have described an example of such a species herein, $\{[\text{PhBP}_3]\text{Fe}^{\text{II}}\equiv\text{N}(1\text{-Ad})\} \{^n\text{Bu}_4\text{N}\}$ (**4.3**), that features a linear Fe-N-C bond angle, a short Fe-N bond length, and a diamagnetic ground state. These features are collectively indicative of significant Fe-N multiple bonding character in the complex. The DFT calculation presented for this system corroborates the d-orbital splitting scheme that we have proposed previously,¹¹ placing three low-lying and largely non-bonding orbitals ($d_{x^2-y^2}$, d_{xy} , d_z^2) at similar energy and well separated from two high-lying orbitals (d_{xz} , d_{yz}) with significant σ and π antibonding contributions (see Figure 8). This orbital arrangement favors a d^6 electronic configuration and additionally accommodates a d^5 configuration, as demonstrated by the relative stability of doublet imides such as complex **2.12**. It is therefore evident that the imide ligand confers a low-spin electronic configuration to both pseudotetrahedral iron(II) and iron(III) centers, at least for [BP₃]Fe systems. As we have recently shown, transforming the imide ligand to a terminal nitride ligand significantly alters the d-orbital splitting scheme.⁶ In the latter case, the a_1 orbital of d_z^2 character is strongly destabilized due to favorable directional overlap with a $2p_z$ orbital at the nitride N-atom. This arrangement favors the d^4 configuration, in accord with our successful characterization of $[\text{PhBP}^{i\text{Pr}}_3]\text{Fe}^{\text{IV}}\equiv\text{N}$.

Addition of one electron to this latter species produces the hypothetical d^5 anion “[PhBP^{iPr}₃]Fe(N)⁻,” which would be characterized by a double (or partial triple) bond due to the population of a strongly antibonding orbital by one electron (Figure 4.8). Needless to say, such a species should be a potent reductant in its own right, and it is therefore not surprising that the reduction of azide **4.1** ultimately leads to an anionic bridged nitride rather than an anionic terminal nitride species. We emphasize that for the d^6 and d^5 imides, and for the d^4 nitride, the Fe-N triple-bond formulation is appropriate under three-fold symmetry. This situation sharply contrasts four-fold symmetric Fe=E species (E = O, N),^{37,38} where the population of π^* antibonding orbitals prohibits the formation of a bonafide triple bond.

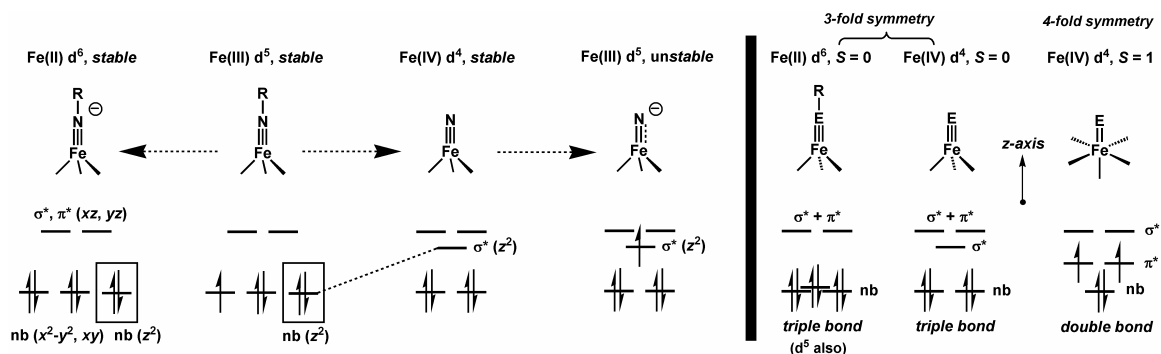


Figure 4.8. (left) Qualitative d-orbital splitting diagrams illustrating the predicted ground-state electronic structures of various $[BP_3]Fe\equiv N_x$ species for d^2 , d^3 , and d^4 configurations. Note that for the imide species an orbital of a_1 symmetry with d_z^2 character lies in the non-bonding region, very close in energy to orbitals with $d_x^2 - y^2$ and d_{xy} character. Therefore, d^6 and d^5 configurations are relatively stable. In contrast, the a_1 orbital is strongly destabilized for a terminal nitride species, $[BP_3]Fe\equiv N$. Therefore, the d^4 configuration is relatively stable whereas the d^5 configuration is destabilized due to population of a high-lying orbital. (right)

Comparison of the d-orbital splitting diagrams anticipated under idealized three-fold and four-fold symmetry. Whereas an Fe≡E triple bond best describes the configurations shown under three-fold symmetry, an Fe=E double bond best describes the configurations shown under four-fold symmetry.

4.4 Experimental Section

4.4.1 General Considerations

General considerations are outlined in Section 3.4.1. Deuterated THF was purchased from Cambridge Isotope Laboratories, Inc. and dried over fine alumina (THF) prior to use.¹⁵N NMR data was acquired on an Inova 500 MHz spectrometer and chemical shifts were referenced to CH₃NO₂ (380 ppm relative to liquid ammonia at 0 ppm). UV/vis/NIR measurements were taken in THF-*d*₈ on a Cary 500 UV/vis/NIR spectrophotometer using a 0.1 cm quartz cell with a Teflon stopper.

4.4.2 Magnetic Measurements

SQUID data for azide **4.1** was acquired from 4–290 K as outlined in Section 2.5.2.

4.4.3 Electrochemical Measurements

Electrochemical procedures are outlined in Section 2.5.4.

4.4.4 DFT Calculations

A hybrid density functional calculation was performed for $\{[\text{PhBP}_3]\text{Fe}\equiv\text{N}(\text{tBu})\}^-$ using the Jaguar package (version 5.0, release 20).³⁹ The calculation employed B3LYP with LACVP** (LACVP**++ for B) as the basis set.⁴⁰ A geometry optimization was carried out using the X-ray coordinates for **2.12** (with all of the carbon atoms of the adamantyl group removed except for those directly attached to the imide nitrogen atom)

as the initial HF guess. No symmetry constraints were imposed and the calculation was performed assuming a singlet electronic ground state.

4.4.5 Starting Materials and Reagents

All reagents were purchased from commercial vendors and used without further purification unless otherwise stated. $[\text{Na}][\text{N}_3]$, $[\text{Na}][^{15}\text{NNN}]$ (Cambridge Isotope Laboratories), and $[\text{K}][\text{NCO}]$ were dried under reduced pressure at 120 °C overnight prior to use. The compounds $[\text{PhBP}_3]\text{FeCl}$ (**2.1**) and $[\text{PhBP}_3]\text{Fe}(\text{PPh}_3)$ (**2.4**) were prepared according to literature procedures.¹¹ Imide **2.12** was prepared according to Section 2.5.8.

4.4.6 Synthesis of Compounds

Synthesis of $\{[\text{PhBP}_3]\text{Fe}(\mu\text{-1,3-N}_3)\}_2$, **4.1:** Chloride **2.1** (1.00 g, 1.28 mmol) was dissolved in acetonitrile (10 mL) with stirring and added to a stirring acetonitrile (5 mL) slurry of $[\text{Na}][\text{N}_3]$ (0.0837 g, 1.28 mmol). The initial red color of the reaction gradually faded as a purple solid precipitated out of the solution. After 24 hours volatiles were removed under reduced pressure, and the solids were extracted with benzene (50 mL), filtered over Celite, and lyophilized. The resulting solid was isolated on a sintered glass frit, washed with ether (2 x 10 mL), petroleum ether (3 x 30 mL), and dried to yield 0.861 g (85%) of a reddish-brown powder. X-ray quality crystals were grown via vapor diffusion of petroleum ether into a benzene solution. IR (KBr/ C_6H_6): $\nu(\text{N}_3) = 2077 \text{ cm}^{-1}$. UV-vis (C_6H_6) λ_{max} , nm (ϵ , $\text{M}^{-1} \text{ cm}^{-1}$): 410 (700). SQUID: $\mu_{\text{eff}} = 4.3 \mu_{\text{B}}$ at 290 K. Evans Method (C_6D_6): $\mu_{\text{eff}} = 4.50 \mu_{\text{B}}$. Anal. Calcd. for $\text{C}_{45}\text{H}_{41}\text{BFeN}_3\text{P}_3$: C, 68.99; H, 5.28; N, 5.36. Found: C, 68.66; H, 5.33; N, 5.34. For **4.1**- ^{15}N : an analogous synthetic procedure employing $[\text{Na}][^{15}\text{NNN}]$ yielded ^{15}N labeled **4.1**. IR (KBr/ C_6H_6): $\nu(\text{N}_3) = 2066 \text{ cm}^{-1}$.

Synthesis of $\{[\text{PhBP}_3\text{Fe}]_2(\mu\text{-N})\}[\text{Na}(\text{THF})_5]$, **4.2:** Azide **4.1** (0.874 g, 1.12 mmol) was dissolved in THF (15 mL) with stirring. To this solution was added 1 equivalent of sodium in the form of a 0.20 weight % Na/Hg amalgam (0.0256 g Na dissolved in 13.5 g Hg). The addition of the amalgam resulted in the vigorous effervescence of N_2 as the color of the reaction solution darkened. After ~ 5 minutes the effervescence had subsided, and the reaction was capped and allowed to stir at room temperature for 8 hours. After this time the reaction was decanted from the amalgam, and volatiles were removed under reduced pressure. The crude solids were extracted with a fresh aliquot of THF (40 mL) and filtered over Celite. Volatiles were again removed under reduced pressure, and the resulting solids were collected on a sintered glass frit and washed with copious amounts of benzene ($\sim 5 \times 30$ mL), petroleum ether (2×15 mL), and dried to obtain 0.546 g (52%) of a brown solid. X-ray quality crystals were grown from a THF/hexanes vapor diffusion chamber while samples for elemental and ^1H NMR analysis were repeatedly crystallized from THF/petroleum ether. ^1H NMR (THF- d_8 , 300 MHz): δ 7.72 (d, $J = 6.0$ Hz, 4H); 7.44 (br s, 24H); 7.12 (t, $J = 7.2$ Hz, 4H); 6.88 (t, $J = 7.2$ Hz, 2H); 6.70 (t, $J = 7.5$ Hz, 12H); 6.53 (t, $J = 7.5$ Hz, 24H); 3.60 (m, 20H, overlaps with residual solvent peaks); 1.78 (m, 20H, overlaps with residual solvent peaks); 1.56 (br s, 12H). $^{31}\text{P}\{^1\text{H}\}$ NMR (THF- d_8 , 121.4 MHz): δ 58.0 (s). UV/vis/NIR (THF- d_8) λ , nm (ϵ , $\text{M}^{-1} \text{cm}^{-1}$): 1266 (943), 1120 (2740), 565 (11 520), 445 (20 530), 390 (21 300). Anal. Calcd. for $\text{C}_{110}\text{H}_{122}\text{B}_2\text{Fe}_2\text{NNaO}_5\text{P}_6$: C, 70.26; H, 6.54; N, 0.74. Found: C, 70.06; H, 6.35; N, 0.82. A sample of ^{15}N enriched **4.2** (50%) was synthesized using an analogous synthetic procedure with **4.1**- ^{15}N . ^{15}N NMR (THF, 50.751 MHz): δ 801 (s).

Synthesis of $\{\text{PhBP}_3\text{Fe}\equiv\text{N}(\text{1-Ad})\}\{\text{Bu}_4\text{N}\}$, **4.3:** Compound **2.12** (0.168 g, 0.189 mmol) was dissolved in THF (5 mL) with stirring. A 0.20 weight % Na/Hg amalgam (0.0043 g Na dissolved in ca. 2.2 g Hg) was added to the THF solution of **2.12**, and the reaction was allowed to stir at room temperature for two hours. The reaction solution was then transferred from the amalgam and stirred in a vial containing $[\text{Bu}_4\text{N}][\text{Br}]$ (0.0606 g, 0.189 mmol) for 4 hours. After this time the volatiles were removed under reduced pressure, and the crude solids were extracted with a fresh aliquot of THF (20 mL) and filtered over a pad of celite. Volatiles were again removed under reduced pressure, and the resulting brown solids were washed with benzene (3 x 10 mL) and dried to obtain 0.141 g (66%) of **4.3**. Crystals suitable for an X-ray diffraction study were grown via vapor diffusion of petroleum ether into a THF solution. ^1H NMR (THF- d_8 , 300 MHz): δ 7.79 (br s, 12H); 7.57 (m, 2H); 7.04 (t, $J = 7.2$ Hz, 2H); 6.67 (m, 18H); 3.07 (m, 8H); 2.15 (s, 6H); 2.07 (s, 3H); 1.78 (m, 6H); 1.57 (m, 8H); 1.35 (m, 8H); 0.98 (t, $J = 7.2$ Hz, 12H, overlaps with ligand methylene resonance at δ 0.94); 0.94 (s, 6H, overlaps with $^n\text{Bu}_4\text{N}^+$ resonance at δ 0.98). $^{31}\text{P}\{^1\text{H}\}$ NMR (THF- d_8 , 121.4 MHz): δ 95.0 (s). $^{11}\text{B}\{^1\text{H}\}$ NMR (THF- d_8 , 128.3 MHz): δ -13.5 (s). UV/vis/NIR (THF- d_8) λ , nm (ϵ , $\text{M}^{-1}\text{cm}^{-1}$): 600 (815), 510 (2112). Anal. Calcd. for $\text{C}_{71}\text{H}_{92}\text{BF}_e\text{N}_2\text{P}_3$: C, 75.26; H, 8.18; N, 2.47. Found: C, 75.15; H, 8.31; N, 2.78.

Synthesis of $[\text{PhBP}_3\text{Fe}(\text{CO})_2(\text{NCO})]$, **4.4:** Compound **4.5** (0.050 g, 0.060 mmol) and $[\text{K}][\text{NCO}]$ (0.049 g, 0.60 mmol) were stirred in THF (5 mL) for 24 hours. After this time volatiles were removed under reduced pressure, and the crude solids were extracted with benzene (5 mL), filtered over celite, and lyophilized to yield 0.038 g (75%) of a yellow solid. ^1H NMR (C_6D_6 , 300 MHz): δ 7.84 (d, $J = 7.2$ Hz, 2H); 7.69 (br s, 8H); 7.55

(t, $J = 7.2$ Hz, 2H); 7.36 (d, $J = 7.2$ Hz, 1H); 7.10 (m, 4H); 6.86 (br s, 14H); 6.72 (m, 4H); 1.83 (br d, $J = 60$ Hz, 4H); 1.56 (d, $J = 14$ Hz, 2H). $^{31}\text{P}\{^1\text{H}\}$ NMR (C_6D_6 , 121.4 MHz): δ 50.4 (t, $J = 58$ Hz, 1P); 27.3 (d, $J = 58$ Hz, 2P). IR (KBr/ C_6H_6): $\nu(\text{CO}) = 2043, 1999\text{ cm}^{-1}$; $\nu(\text{NCO}) = 2195, 2224\text{ cm}^{-1}$. Anal. Calcd. for $\text{C}_{48}\text{H}_{41}\text{BFeNO}_3\text{P}_3$: C, 68.68; H, 4.92; N, 1.67. Found: C, 69.01; H, 5.23; N, 2.01.

Synthesis of $[\text{PhBP}_3]\text{Fe}(\text{CO})_2\text{Cl}$, 4.5: Chloride **2.1** (0.200 g, 0.257 mmol) was stirred in benzene (10 mL) in a 50 mL Schlenk flask. The solution was frozen, and the atmosphere was evacuated and replaced with one atmosphere of CO. The reaction was then allowed to warm to room temperature and stirred for an additional 30 minutes. After this time the volatiles were removed under reduced pressure, yielding an essentially quantitative amount of a golden solid. ^1H NMR (C_6D_6 , 300 MHz): δ 7.87 (m, 10H); 7.56 (t, $J = 7.2$ Hz, 2H); 7.35 (t, $J = 6.0$ Hz, 1H); 7.20 (m, $J = 7.2$ Hz, 4H); 6.84 (m, 14H); 6.74 (m, 4H); 1.91 (br d, $J = 57$ Hz, 4H); 1.62 (d, $J = 15$ Hz, 2H). $^{31}\text{P}\{^1\text{H}\}$ NMR (C_6D_6 , 121.4 MHz): δ 54.7 (t, $J = 53$ Hz, 1P); 25.2 (d, $J = 53$ Hz, 2P). $^{11}\text{B}\{^1\text{H}\}$ NMR (C_6D_6 , 128.3 MHz): δ -13.9 (s). IR (KBr/ C_6H_6): $\nu(\text{CO}) = 2039, 1997\text{ cm}^{-1}$. ES-MS: calcd. for $\text{C}_{47}\text{H}_{41}\text{BClFeO}_2\text{P}_3$ (M) $^+$: 833 m/z, found ($\text{M} - \text{Cl}$) $^+$ 797 m/z. Anal. Calcd. for $\text{C}_{47}\text{H}_{41}\text{BClFeO}_2\text{P}_3$: C, 67.78; H, 4.96. Found: C, 67.45; H, 5.13.

The reaction of 4.2 with CO: Nitride **4.2** (0.0083 g, 0.004 mmol) was dissolved in THF in a sealable NMR tube. The resulting solution was frozen, and the N_2 atmosphere was evacuated and replaced with one atmosphere of CO. The NMR tube was shaken periodically over a period of 10 minutes at which time a crude ^{31}P NMR spectrum confirmed the presence of **4.4**. After this time volatiles were removed under reduced pressure, and both ^1H NMR (C_6D_6) and IR analysis (KBr/ C_6H_6) confirmed the presence

of $[\text{PhBP}_3]\text{Fe}(\text{CO})_2$ ¹¹ as the major product and **4.4** as the minor product. Addition of a hexamethylbenzene internal standard to this ¹H NMR sample demonstrated that **4.4** was produced in ca. 25% yield.

The reaction of 4.2 with HCl: Nitride **4.2** (0.030 g, 0.0160 mmol) was dissolved in 1 mL of THF in a sealable NMR tube. The solution was cooled to -35 °C, and 3 equivalents of HCl (46 μL of a 1 M solution in Et₂O diluted in 0.25 mL THF) cooled to -35 °C were added. The reaction was then allowed to warm to room temperature. After 30 minutes the reaction volatiles were vacuum transferred into 5 mL of a 1 M solution of HCl in Et₂O. Once the transfer was complete, the HCl solution was stirred at room temperature for about 30 minutes. At this point a small amount of precipitate was evident, and the volatiles were removed under reduced pressure. The resulting residue was dissolved in DMSO-*d*₆, and the presence of $[\text{NH}_4][\text{Cl}]$ was confirmed by a triplet at δ 7.15 ppm (t, $J = 51$ Hz, 4H), which was integrated versus an internal ferrocene standard.⁶ Two independent runs provided an 80% and a 95% yield of NH₃, respectively. The remaining solids from the original reaction were dissolved in benzene-*d*₆, and chloride **2.1** was observed to be the major (> 80%) iron-containing product by ¹H NMR spectroscopy.

4.4.7 X-ray Experimental Data

Crystallographic procedures are outlined in Section 2.5.8. Crystallographic data are summarized in Table 4.1. Crystals of imide **2.12** were obtained as outlined in Section 2.5.8.

Table 4.1. Crystallographic data for $\{[\text{PhBP}_3]\text{Fe}(\mu\text{-}1,3\text{-N}_3)\}_2$ (**4.1**), $[\{[\text{PhBP}_3]\text{Fe}\}_2(\mu\text{-N})][\text{Na}(\text{THF})_5]$ (**4.2**), $\{[\text{PhBP}_3]\text{Fe}\equiv\text{N}(1\text{-Ad})\}\{\text{Bu}_4\text{N}\}$ (**4.3**), and $[\text{PhBP}_3]\text{Fe}\equiv\text{N}(1\text{-Ad})$ (**2.12**).

	monomer 4.1 ·C ₆ H ₆	4.2 ·THF	2.12 ·THF
chemical formula	C ₅₁ H ₄₇ BFeN ₃ P ₃	C ₁₁₄ H ₁₃₀ B ₂ Fe ₂ NNa O ₆ P ₆	C ₇₅ H ₁₀₀ BFeN ₂ OP ₃
fw	861.49	1952.32	1205.14
<i>T</i> (°C)	-177	-177	-177
λ (Å)	0.71073	0.71073	0.71073
<i>a</i> (Å)	13.0738(10)	16.7910(8)	12.173(3)
<i>b</i> (Å)	14.2209(11)	13.7352(6)	14.051(4)
<i>c</i> (Å)	14.6878(12)	43.299(2)	22.131(6)
α (°)	118.2270(10)	90	71.610(4)
β (°)	95.2290(10)	93.6530(10)	79.790(4)
γ (°)	111.0900(10)	90	68.373(4)
<i>V</i> (Å ³)	2128.4(3)	9965.8(8)	3331.1(14)
space group	P-1	P2(1)/c	P-1
<i>Z</i>	2	4	2
<i>D</i> _{calc} (g/cm ³)	1.344	1.301	1.202
μ (cm ⁻¹)	5.08	4.49	3.44
R1, wR2 ^a (<i>I</i> > 2σ(<i>I</i>))	0.0396, 0.0858	0.0650, 0.0940	0.0470, 0.0972

^a $R1 = \Sigma||F_o| - |F_c||/\Sigma|F_o|$, $wR2 = \{\Sigma[w(F_o^2 - F_c^2)^2]/\Sigma[w(F_o^2)^2]\}^{1/2}$

Table 4.1 cont.

2.12	
chemical formula	C ₅₅ H ₅₆ BFeNP ₃
fw	890.58
<i>T</i> (°C)	-177
λ (Å)	0.71073
<i>a</i> (Å)	16.4143(15)
<i>b</i> (Å)	14.1225(13)
<i>c</i> (Å)	20.7686(19)
α (°)	90
β (°)	109.186(2)
γ (°)	90
<i>V</i> (Å ³)	4547.0(7)
space group	P2(1)/n
<i>Z</i>	4
<i>D</i> _{calc} (g/cm ³)	1.301
μ (cm ⁻¹)	4.76
R1, wR2 ^a (<i>I</i> > 2 σ (<i>I</i>))	0.0489, 0.0982

References Cited

¹ (a) Huniar, U.; Ahlrichs, R.; Coucouvanis, D. *J. Am. Chem. Soc.* **2004**, *126*, 2588. (b) Hinnemann, B.; Nørskov, J. K. *J. Am. Chem. Soc.* **2004**, *126*, 3920. (c) Lee, H.-I.; Benton, P. M. C.; Laryukhin, M.; Igarashi, R. Y.; Dean, D. R.; Seefeldt, L. C.; Hoffman, B. M. *J. Am. Chem. Soc.* **2003**, *125*, 5604. (d) Schimpl, J.; Petrilli, H. M.; Blochl, P. E. *J. Am. Chem. Soc.* **2003**, *125*, 15772. (e) Cao, Z.; Zhou, Z.; Wan, H.; Zhang, Q.; Thiel, W. *Inorg. Chem.* **2003**, *42*, 6986. (f) Hinnemann, B.; Nørskov, J. K. *J. Am. Chem. Soc.* **2003**, *125*, 1466. (g) Dance, I. *Chem. Commun.* **2003**, 324.

² Einsle, O.; Tezcan, F. A.; Andrade, S. L. A.; Schmid, B.; Yoshida, M.; Howard, J. B.; Rees, D. C. *Science* **2002**, *297*, 1696.

³ Lee, S. C.; Holm, R. H. *Chem. Rev.* **2004**, *104*, 1135.

⁴ Ertl, G. *Chem. Rec.* **2001**, *1*, 33.

⁵ For examples of structurally characterized Fe-N-Fe linkages, see: (a) Justel, T.; Muller, M.; Weyhermuller, T.; Kressl, C.; Bill, E.; Hildebrandt, P.; Lengen, M.; Grodzicki, M.; Trautwein, A. X.; Nuber, B.; Wieghardt, K. *Chem.-Eur. J.* **1999**, *5*, 793. (b) Kienast, A.; Homborg, H. Z. *Anorg. Allg. Chem.* **1998**, *624*, 233. (c) Moubaraki, B.; Benlian, D.; Baldy, A.; Pierrot, M. *Acta Crystallogr., Sect. C* **1989**, *45*, 393. (d) Scheidt, W. R.; Summerville, D. A.; Cohen, I. A. *J. Am. Chem. Soc.* **1976**, *98*, 6623. (e) Summerville, D. A.; Cohen, I. A. *J. Am. Chem. Soc.* **1976**, *98*, 1747.

⁶ Betley, T. A.; Peters, J. C. *J. Am. Chem. Soc.* **2004**, *126*, 6252.

⁷ High-spin iron(V) terminal nitrides have been reported on the basis of spectroscopic data at low temperatures. See: (a) Meyer, K. M.; Eckhard, B.; Mienert, B.;

Weyhermuller, T.; Wieghardt, K. *J. Am. Chem. Soc.* **1999**, *121*, 4859. (b) Wagner, W.-D.; Nakamoto, K. *J. Am. Chem. Soc.* **1989**, *111*, 1590.

⁸ (a) Thomas, J. C.; Peters, J. C. *Inorg. Synth.* **2004**, *34*, 8. (b) Barney, A. A.; Heyduk, A. F.; Nocera, D. G. *Chem. Commun.* **1999**, 2379.

⁹ Betley, T. A.; Peters, J. C. *J. Am. Chem. Soc.* **2003**, *125*, 10782.

¹⁰ Brown, S. D.; Peters, J. C. *J. Am. Chem. Soc.* **2004**, *126*, 4538.

¹¹ Brown, S. D.; Betley, T. A.; Peters, J. C. *J. Am. Chem. Soc.* **2003**, *125*, 322.

¹² For other examples of chemistry featuring [PhBP^{iPr}₃], see: (a) Turculet, L.; Feldman, J. D.; Tilley, T. D. *Organometallics* **2004**, *23*, 2488. (b) Betley, T. A.; Peters, J. C. *Inorg. Chem.* **2003**, *42*, 5074. (c) Turculet, L.; Feldman, J. D.; Tilley, T. D. *Organometallics* **2003**, *22*, 4627.

¹³ For other examples of chemistry featuring [PhBP₃], see: (a) Jenkins, D. M.; Peters, J. C. *J. Am. Chem. Soc.* **2003**, *125*, 11162. (b) Jenkins, D. M.; Betley, T. A.; Peters, J. C. *J. Am. Chem. Soc.* **2002**, *124*, 11238. (c) Jenkins, D. M.; Di Bilio, A. J.; Allen, M. J.; Betley, T. A.; Peters, J. C. *J. Am. Chem. Soc.* **2002**, *124*, 15336. (d) Feldman, J. D.; Peters, J. C.; Tilley, T. D. *Organometallics* **2002**, *21*, 4065. (e) Feldman, J. D.; Peters, J. C.; Tilley, T. D. *Organometallics* **2002**, *21*, 4050.

¹⁴ (a) Mindiola, D. J.; Cummins, C. C. *Angew. Chem., Int. Ed.* **1998**, *37*, 945. (b) Carpino, L. A.; Padykula, R. E.; Barr, D. E.; Hall, F. H.; Krause, J. G.; Dufresne, R. F.; Thoman, C. J. *J. Org. Chem.* **1988**, *53*, 2565.

¹⁵ (a) Du Bois, J.; Tomooka, C. S.; Hong, J.; Carreira, E. M. *Acc. Chem. Res.* **1997**, *30*, 364. (b) Nugent, W. A.; Mayer, J. M. *Metal-Ligand Multiple Bonds*; Wiley & Sons: New York, 1988; p 76. (c) LaMonica, G.; Cenini, S. *J. Chem. Soc., Dalton Trans.* **1980**, 1145.

-
- ¹⁶ Duimstra, J.; Peters, J. C. *Unpublished Results*.
- ¹⁷ Nakamoto, K. *Infrared and Raman Spectra of Inorganic and Coordination Compounds. Part B: Applications in Coordination, Organometallic, and Bioinorganic Chemistry*, 5th ed.; Wiley & Sons: New York, 1997; p 124.
- ¹⁸ (a) Sur, S. K. *J. Magn. Reson.* **1989**, *82*, 169. (b) Evans, D. F. *J. Chem. Soc.* **1959**, 2003.
- ¹⁹ Daida, E. J.; Peters, J. C. *Inorg. Chem.* **2004**, *43*, 7474. Also see ref 12c for a [PhBPⁱPr₃]Fe^{II}-SiR₃ example.
- ²⁰ To the best of our knowledge, examples of (μ -1,3) bridging azide systems for iron have yet to be reported. For examples of (μ -1,1) systems, see: (a) Clemente-Juan, J. M.; Mackiewicz, C.; Verelst, M.; Dahan, F.; Bousseksou, A.; Sanakis, Y.; Tuchagues, J.-P. *Inorg. Chem.* **2002**, *41*, 1478. (b) Reddy, K. R.; Rajasekharan, M. V.; Tuchagues, J.-P. *Inorg. Chem.* **1998**, *37*, 5978. (c) De Munno, G.; Poerio, T.; Viau, G.; Julve, M.; Lloret, F. *Angew. Chem., Int. Ed. Engl.* **1997**, *36*, 1459. (d) De Munno, G.; Poerio, T.; Viau, G.; Julve, M.; Lloret, F. *Chem. Commun.* **1996**, 2587.
- ²¹ A τ value of 1 corresponds to an ideal trigonal bipyramidal geometry, while a τ value of 0 corresponds to an ideal square pyramidal geometry. See: Addison, A. W.; Rao, T. N.; Reedijk, J.; van Rin, J.; Verschoor, G. C. *J. Chem. Soc., Dalton Trans.* **1984**, 1349.
- ²² The decrease in χ_M^*T below 16 K for [α -(Me₃tacn)₂(cyclam)NiMo₂(CN)₆]I₂, which features a ferromagnetically coupled $S = 4$ electronic configuration, was also attributed to zero-field splitting. See: Shores, M. P.; Sokol, J. J.; Long, J. R. *J. Am. Chem. Soc.* **2002**, *124*, 2279. For a more detailed discussion concerning the magnetism of differous bridged

systems, see: Hendrich, M. P.; Day, E. P.; Wang, C.-P.; Synder, B. S.; Holm, R. H.; Munck, E. *Inorg. Chem.* **1994**, *33*, 2848 and references therein.

²³ Verma, A. K.; Nazif, T. N.; Achim, C.; Lee, S. C. *J. Am. Chem. Soc.* **2000**, *122*, 11013.

²⁴ We have considered the presence of a (μ -NH) functionality instead of a (μ -N) ligand. However, IR studies of **4.2** as both a solution (THF) and a solid (Nujol, KBr pellet) provide no evidence for an N-H vibration. Additionally, it is not possible to assign formal iron oxidation states with a (μ -NH) ligand and still maintain a diamagnetic manifold while accounting for all charges.

²⁵ Caselli, A.; Solari, E.; Scopelliti, R.; Floriani, C.; Re, N.; Rizzoli, C.; Chiesi-Villa, A. *J. Am. Chem. Soc.* **2000**, *122*, 3652.

²⁶ (a) Glidewell, C.; Holden, H. D. *J. Organomet. Chem.* **1982**, *226*, 171. (b) Canziani, F.; Garlaschelli, L.; Malatesta, M. C.; Albinati, A. *J. Chem. Soc., Dalton Trans.* **1981**, 2395.

²⁷ (a) Shannon, R. D. *Acta. Crystallogr.* **1976**, *A32*, 751. (b) Shannon, R. D.; Prewitt, C. T. *Acta. Crystallogr.* **1969**, *B25*, 925.

²⁸ See, for example: (a) Cherry, J.-P. F.; Stephens, F. H.; Johnson, M. J. A.; Diaconescu, P. L.; Cummins, C. C. *Inorg. Chem.* **2001**, *40*, 6860. (b) Tsai, Y.-C.; Johnson, M. J. A.; Mendiola, D. J.; Cummins, C. C. *J. Am. Chem. Soc.* **1999**, *121*, 10426. (c) Banaszak Holl, M. M.; Kersting, M.; Pendley, B. D.; Wolczanski, P. T. *Inorg. Chem.* **1990**, *29*, 1518.

²⁹ Vela, J.; Stoian, S.; Flaschenriem, C. J.; Munck, E.; Holland, P. L. *J. Am. Chem. Soc.* **2004**, *126*, 4522.

³⁰ For an example of a d⁶ iridium imide, see: Glueck, D. S.; Wu, J.; Hollander, F. J.; Bergman, R. G. *J. Am. Chem. Soc.* **1991**, *113*, 2041.

³¹ Orpen, A. G.; Connelly, N. G. *Organometallics* **1990**, *9*, 1206.

³² Bianchini, C.; Laschi, F.; Masi, D.; Ottaviani, F. M.; Pastor, A.; Peruzzini, M.; Zanello, P.; Zanobini, F. *J. Am. Chem. Soc.* **1993**, *115*, 2723.

³³ For example, the $^5E \rightarrow ^5T_2$ transition for $\text{Fe}(\text{HMPA})_4^{2+}$ (HMPA = hexamethylphosphoramide) occurs at 6950 cm^{-1} . See: Lever, A. B. P. *Inorganic Electronic Spectroscopy*, 2nd ed.; Elsevier: Amsterdam, 1984; p 461.

³⁴ For an example of a bridged N_4 ligand, see: Mass, V. W.; Kujanek, R.; Baum, G.; Dehnicke, K. *Angew. Chem., Int. Ed. Engl.* **1984**, *23*, 149. For an example of a terminal N_4 ligand, see: Huynh, M. H. V.; Baker, R. T.; Jameson, D. L.; Labouriau, A.; Meyer, T. *J. Am. Chem. Soc.* **2002**, *124*, 4580.

³⁵ Consistent with this suggestion is that the well-defined Fe(IV) nitride species $[\text{PhBP}^{i\text{Pr}}_3]\text{Fe}\equiv\text{N}$ (ref 6) is reduced by CO in benzene to produce a mixture of two diamagnetic iron(II) isocyanates: $[\text{PhBP}^{i\text{Pr}}_3]\text{Fe}(\text{NCO})(\text{CO})$ and $[\text{PhBP}^{i\text{Pr}}_3]\text{Fe}(\text{NCO})(\text{CO})_2$. This transformation and further reactivity studies pertaining to $[\text{PhBP}^{i\text{Pr}}_3]\text{Fe}\equiv\text{N}$ will be elaborated in due course.

³⁶ Yandulov, D. V.; Schrock, R. R. *J. Am. Chem. Soc.* **2002**, *124*, 6252.

³⁷ Rohde, J. U.; In, J.-H.; Lim, M. H.; Brennessel, W. W.; Bukowski, M. R.; Stubna, A.; Munck, E.; Nam, W.; Que, L., Jr. *Science* **2003**, *299*, 1037. See also ref 11.

³⁸ Costas, M.; Mehn, M. P.; Jensen, M. P.; Que, L., Jr. *Chem. Rev.* **2004**, *104*, 939.

³⁹ Jaguar 5.0, Schrodinger, LLC, Portland, Oregon, 2002.

⁴⁰ Lee, C.; Yang, W.; Parr, R. G. *Phys. Rev. B* **1988**, *37*, 785-789.